MOTION BLUR ESTIMATION AT CORNERS

Giacomo Boracchi and Vincenzo Caglioti
Dipartimento di Elettronica e Informazione, Politecnico di Milano, Via Ponzio, 34/5- 20133 MILANO
boracchi@elet.polimi.it, caglioti@elet.polimi.it

Keywords: Point Spread Function Parameter Estimation, Motion Blur, Space Varying Blur, Blurred Image Analysis, Optical Flow.

Abstract: In this paper we propose a novel algorithm to estimate motion parameters from a single blurred image, exploiting geometrical relations between image intensities at pixels of a region that contains a corner. Corners are significant both for scene and motion understanding since they permit a univocal interpretation of motion parameters. Motion parameters are estimated locally in image regions, without assuming uniform blur on image so that the algorithm works also with blur produced by camera rotation and, more in general, with space variant blur.

1 INTRODUCTION

Motion estimation is a key problem both in image processing and computer vision. It is usually performed comparing frames from a video sequence or a pair of still images. However, in case of fast motion or long exposure images, motion can be also estimated by analyzing only a single blurred image. Algorithms that consider one image have to face a more challenging problem, because little information is available, since both image content and blur characteristics are unknown.
In this paper we introduce an algorithm to estimate motion from a single blurred image, exploiting motion direction and length at image corners. Several algorithms that estimate motion blur from a single image have been proposed; most of them process the image Fourier transform, assuming uniform blur (Choi et al., 1998), (Kawamura et al., 2002). Rekletis (Rekleitis, 1996) estimates locally motion parameters from a blurred image by defining an image tessellation, and then analyzing Fourier transform of each region separately. However frequency domain based algorithms are not able to manage blur when motion parameters are varying through the image. Moreover, motion estimation from Fourier domain is particularly difficult at image corners because Fourier coefficients are mostly influenced by the presence of edges than from blur.
Our algorithm considers image regions containing a blurred corner and estimates motion direction and length by exploiting geometrical relations between pixels intensity values. Beside blind deconvolution, motion estimation from a single image has been addressed for several other purposes. Rekleitis estimates the optical flow (Rekleitis, 1996), Lin determines vehicle and ball speed (Lin and Chang, 2005), (Lin, 2005) and more recently Klein (Klein and Drummond, 2005) suggested a visual gyroscope based on estimation of rotational blur.
The paper is organized as follows: in Section 2 the blur model and the corner model are introduced, in Section 3 we present the algorithm core idea and in Section 4 we describe a robust solution based on a voting algorithm. Section 5 describes the algorithm details and presents experimental results.

2 PROBLEM FORMULATION

Our goal is to estimate blur direction and extent at some salient points, which are pixels where it is possible to univocally interpret the motion. For example, pixels where the image is smooth as well as

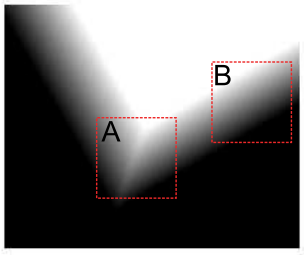

Figure 1: Blurred corner synthetically generated.

pixels along a blurred edge do not allow an univocal motion interpretation: given a blurred edge or a blurred smooth area there are potentially infinite scene displacements that could have caused the same blur (see region B in Figure 1). Corners, instead, offer a clear interpretation of motion direction and extent and that's the reason why we design an algorithm to estimate motion specifically at corners. We consider image I modelled as follows

$$I(\mathbf{x}) = K\big(y+\xi\big)(\mathbf{x}) + \eta(\mathbf{x}), \quad \mathbf{x} = (x_1, x_2) \qquad (1)$$

where $\mathbf{x}$ is a multi index representing image coordinates varying on a discrete domain X, y is the original and unknown image and K is the blur operator. We introduce two different sources of white noise, ξ and η. In our model η represents electronic and quantization noise, while ξ has been introduced to attenuate differences between corners in real images and the binary corner model that we present in the next section. Therefore ξ plays a crucial role only when a region containing a corner is analyzed.

2.1 The Blur Model

Here we model the blur operator K on the whole image, so that we do not need to consider ξ which is relevant only at image corners.
Our goal is to determine the blur operator K which can be written as (Bertero and Boccacci, 1998)

$$K\big(y\big)(\mathbf{x}) = \int_X k(\mathbf{x},\mu) y(\mu) d\mu. \qquad (2)$$

Usually, K is considered space invariant, so that equation (2) becomes a convolution with a kernel v, called point spread function (PSF)

$$K\big(y\big)(\mathbf{x}) = \int_X v(\mathbf{x}-\mu) y(\mu)\, d\mu = (v \star y)(\mathbf{x}). \qquad (3)$$

This assumption is too restrictive for our purpose, because often scene points follow different trajectories with respect to the camera viewpoint and are indeed differently blurred. Equation (3) does not concern, for instance, scenes where there are objects following different trajectories, scenes with a moving target on a still background and static scenes captured by a rotating camera.

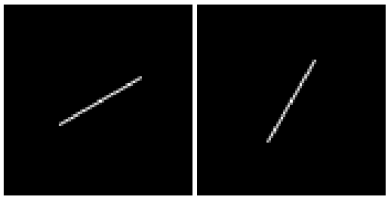

Figure 2: Example of motion blur psf with direction 30 and 60 degrees respectively and length 30 pixels.

On the other hand, solving (2) is a difficult inverse problem: to reduce its complexity we assume that the blur functional K is locally approximated as a shift invariant blur, i.e.
$\forall \mathbf{x}_0 \in X$, $\exists U_0 \subset X$, $x_0 \in U_0$ and a PSF v_0 such that

$$K\big(y\big)(\mathbf{x}) \approx \int_X v_0(\mathbf{x}-\mu) y(\mu) d\mu \quad \forall \mathbf{x} \in U_0. \qquad (4)$$

Furthermore, we consider only motion blur PSF defined over an 1-D linear support: they can be written as

$$v_0 = R_{(\theta)}\big(s_l\big)(\mathbf{x}) \quad \theta \in [0, 2\pi], l \in \mathbb{N}$$

$$s_l(x_1,x_2) = \begin{cases} 1/(2l+1), & -l \le x_1 \le l \\ & x_2 = 0 \\ 0, & else \end{cases}$$

where θ and l are motion direction and length respectively and $R_{(\theta)}\big(s_l\big)$ is function s_l rotated by θ degrees on X . Figure 2 shows examples of motion blur PSF.

2.2 The Corner Model

Our corner model relies on two assumptions. Firstly, we assume that y is a grayscale image or, equivalently, an image plane in a color representation which is constant at corner pixels and at background pixels. This means that given $D \subset X$, neighborhood of an image corner, we have $y(D) = \{b, c\}$, where b and c are the image values for the background and for the corner, respectively. Moreover, the sets of pixels belonging to the background $B = y^{-1}(\{b\})$ and the set of pixels belonging to the corner $C = y^{-1}(\{c\})$, have to be separated by two straight segments (having a common endpoint). Figure 3 shows the corner model.
Then, let us define $\tilde{v}$ as the corner displacement vec-

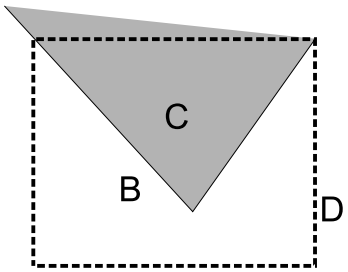

Figure 3: The Corner Model.

tor: this vector has the origin at image corner and direction θ and length l equal to direction and length of the PSF v_0 which locally approximates the blur operator. Let γ be the angle between a reference axis and the corner bisecting line, let α be the corner angle, and θ be the angle between $\tilde{v}$ and the reference axis, then

$$\theta \in [\gamma - \alpha/2, \gamma + \alpha/2] + k\pi \quad k \in \mathbb{N}.$$

Figure 4.**a** shows a corner displacement vector satisfying this assumption, while Figure 4.**b** a corner that does not.

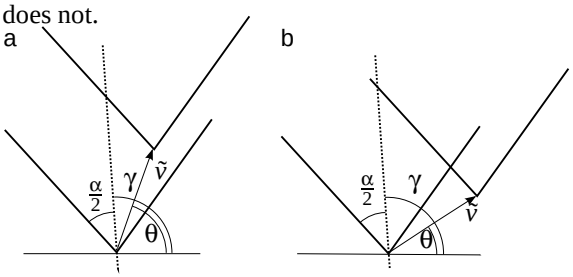

Figure 4: Two possible cases for corner displacements, **a** agrees with our model while **b** does not.

3 PROBLEM SOLUTION

In this section we derive the core equations for motion estimation at a blurred corner that satisfies assumptions of Sections 2.1 and 2.2.
We first consider noise η only, then we exploit how ξ corrupts the proposed solution.

3.1 Binary Corners

Let us examine an image region containing a binary corner, like the one depicted in Figure 3, and let us assume that noise ξ is null. Let d_1 and d_2 be the first order derivative filters w.r.t. x_1 and x_2. The image gradient is defined as

$$\nabla I(\mathbf{x}) = \begin{bmatrix} I_1(\mathbf{x}) \\ I_2(\mathbf{x}) \end{bmatrix} = \nabla K(y)(\mathbf{x}) + \nabla \eta(\mathbf{x}),$$

where $I_1 = (I \star d_1)$ and $I_2 = (I \star d_2)$.
If $\Delta = |c - b|$ is the image intensity difference between the corner and the background, it follows, as illustrated in Figure 5, that

$$\Delta = \tilde{v} \cdot \nabla K(y)(\mathbf{x}), \ \forall \mathbf{x} \in D_0, \qquad (5)$$

where $D_0 = \{\mathbf{x} \in D \,|\, \nabla K(y)(\mathbf{x}) \neq [0,0]^T\}$.
Equation (5) is undeterminate as we do not know Δ and $K(y)$ but only I, which is corrupted by η.
Similar situations can be solved taking into account, $\forall \mathbf{x} \in D_0$, several instances of (5), evaluated at neighboring pixels.

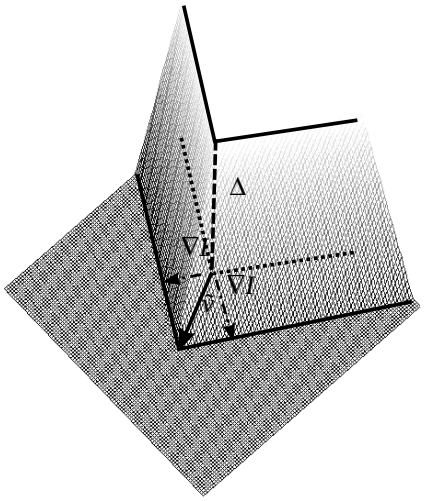

Figure 5: Intensity values of in box A of Figure 1.

We call w a window described by its weight w_i, $-n < i < n$, and we solve the following system

$$A(\mathbf{x})\,\tilde{v} = \Delta\,[w_{-n}, ..., w_0, ..., w_n]^T \qquad (6)$$

where A is defined as

$$A(\mathbf{x}) = \begin{bmatrix} w_{-n}\nabla I(\mathbf{x}_{-n})^T \\ ... \\ w_0 \nabla I(\mathbf{x})^T \\ ... \\ w_n \nabla I(\mathbf{x}_n)^T \end{bmatrix}.$$

In our experiment we choose w as a squared window having gaussian distributed weights.
A solution of system (6) is given by $\tilde{v}$

$$\tilde{v} = \arg\min_v \left\| A(\mathbf{x})\,v - \Delta\,[w_{-n}, ..., w_0, ..., w_n]^T \right\|_2 \qquad (7)$$

which yields

$$\tilde{v} = H^{-1}(\mathbf{x})\,A^T(\mathbf{x})\,[w_{-n}, ..., w_0, ..., w_n] \qquad (8)$$

$$H = \begin{bmatrix} \sum_i w_i^2 I_1(\mathbf{x}_i)^2 & \sum_i w_i^2 I_2(\mathbf{x}_i) I_1(\mathbf{x}_i) \\ \sum_i w_i^2 I_2(\mathbf{x}_i) I_1(\mathbf{x}_i) & \sum_i w_i^2 I_2(\mathbf{x}_i)^2 \end{bmatrix}.$$

H corresponds to Harris Matrix (Harris and Stephens, 1988), whose determinant and trace are used as corner detectors in many feature extraction algorithms, see (Mikolajczyk et al., 2005).
If w does not contain any image corner, H is singular and consequently the system (8) does not admit a unique solution. Therefore, when the window w intersects only one blurred edge (like region B in Figure 1), system (8) admits an infinite number of solutions and the motion parameters can not be estimated.
On the contrary, H is nonsingular when w intersects

two blurred edges (like box A in Figure 1) and in this case the system (8) can be univocally solved.
The least square solution (8) performs optimally in case of gaussian white noise. Here we assume that η is white noise, without specifying any distribution because $\nabla\eta$ would not be white anymore. However, in case of noise with standard deviation significantly smaller than Δ, equation (8) represent a suboptimal solution.

3.2 Noisy Corners

The proposed algorithm works when y contains a binary corner, that takes only two intensity values. These *cartoon world* corners are far from being similar to corners of real images. It is reasonable to expect corners to be distinguishable from their background, but hardly they would be uniform. More often their intensity values would be varying, for example, as there are texture or details. However, since the observed image I is blurred, we do not expect a big difference between a blurred texture and a blurred white noise ξ, added on a blurred corner.
Let then consider how equation (5) changes if $\xi \neq 0$. We have

$$\nabla I(\mathbf{x}) = \nabla K\big(y\big)(\mathbf{x}) + \nabla K\big(\xi\big)(\mathbf{x}),$$

and (5) holds for $\nabla K\big(y\big)(\mathbf{x})$, while it does not for $\nabla K\big(\xi\big)(\mathbf{x})$.
However the blur operator $K\big(\xi\big)$, which is locally a convolution with a PSF, produces a correlation of ξ samples along the motion direction (Yitzhaky and Kopeika, 1996), so that

$$\nabla K\big(\xi\big)(\mathbf{x}) \cdot \tilde{v} \approx 0, \tag{9}$$

which means that the more blur induces correlation among random values of ξ, the more our algorithm will work with corners which are not binary.

4 ROBUST SOLUTION

Although the equation (9) assures that the proposed algorithm would work for most of pixels, even in presence of noise ξ, we expect that outliers would heavily influence the solution (8), since it is an ℓ^2 norm minimization (7).
Beside pixels where $\nabla K\big(\xi\big)(\mathbf{x}) \cdot \tilde{v} \neq 0$ there could be several other noise factors that are not considered in our model but that we should be aware of. For example compressed images often present artifacts at edges such as aliasing and blocking, corners on y are usually smoothed and edges are not perfectly straight lines.
However, if we assume that outliers are a relatively small percentage of pixels, we can still obtain a reliable solution using a robust technique.
We do not look for a vector $\tilde{v}$ that satisfy the equation (5) at each pixel or that minimize the ℓ^2 error norm (7): rather we look for a value of $\tilde{v}$ that satisfies a significant percentage of equations in system (6), disregarding how $\tilde{v}$ is far from the solution of the remaining equations.

4.1 The Voting Approach

If we define, for every pixel, the vector $N(\mathbf{x})$ as

$$N(\mathbf{x}) = \frac{\nabla I(\mathbf{x})}{||\nabla I(\mathbf{x})||^2}\,\Delta, \tag{10}$$

we have that $N(\mathbf{x})$ corresponds to the $\tilde{v}$ component along $\nabla I(\mathbf{x})$ direction, $\forall \mathbf{x} \in D_0$.
The endpoint of any vector $\tilde{v}$, solution of (5), lies on the straight line perpendicular to $N(\mathbf{x})$, going through its endpoint. Then, the locus $\ell_{\mathbf{x}}(\mathbf{u})$ of the possible $\tilde{v}$ endpoints, compatible with a given datum $\nabla I(\mathbf{x})$, is a line (see Figure 6).

As in usual Hough approaches, the 2-D parameter space of $\tilde{v}$ endpoints is subdivided into cells of suitable size (e.g. 1 pixel); a vote is assigned to any cell that contains (at least) a value of $\tilde{v}$ satisfying an instance of equation (5). The most voted cells represent values of $\tilde{v}$ that satisfy a significant number of equations (6).

4.2 Neighborhood Construction

In order to reduce the approximation errors due to the discrete parameter space and to take into account $\nabla\eta$, we assign a full vote (e.g 1) to each parameter pairs that solve (5), (the line of Figure 6), and a fraction of vote to the neighboring parameter pairs.
We define the following function

$$\ell(u_1,u_2) = exp\Big[-\Big(\frac{u_2}{1+k|u_1|\sigma_{\nabla\eta}}\Big)^2\Big], \tag{11}$$

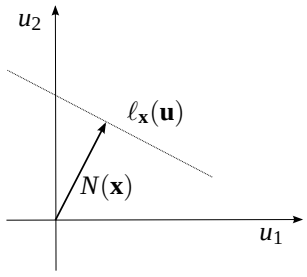

Figure 6: $\ell(\mathbf{x})$ set of possible endpoint for $\tilde{v}$.

where $\sigma_{\nabla\eta}$ is $\nabla\eta$ standard deviation and k is a tuning parameter. ℓ has the following properties: it is constant and equal to 1 on u_1 axis, (i.e. $\ell(u_1,0)=1$), and when evaluated on a vertical line, ($u_1 = const$), it is a gaussian function having standard deviation that depends on $|u_1|$, i.e. $\ell(u_1,u_2) = N(0,1+k|u_1|\sigma_{\nabla\eta})(u_2)$.
We select this function as a prototype of the vote map, given $\nabla I(\mathbf{x})$, the votes distributed in the parameter space are the values of an opportunely translated and scaled version of $\ell(u_1,u_2)$. The straight line of Figure 6, $\ell_{\mathbf{x}}(\mathbf{u})$, is therefore replaced by function ℓ rotated by $(\frac{\pi}{2}-\theta)$ degrees and translated so that its origin is in $N(\mathbf{x})$ endpoint, i.e.

$$\ell_{\mathbf{x}}(\mathbf{u}) = R_{(\frac{\pi}{2}-\theta)}\big(\ell\big)(\mathbf{u}-N(\mathbf{x}))\,, \qquad (12)$$

where θ is $\nabla I(\mathbf{x})$ direction and $R_{(\frac{\pi}{2}-\theta)}$ is the rotation of $(\frac{\pi}{2}-\theta)$ degrees.
In such a way, we give a full vote to parameter pairs which are exact solutions of (5) and we increase the spread of votes as the distance from $N(\mathbf{x})$ endpoint increases.
Figure $7(a)$ shows how votes are distributed in parameter space for a vector $N(\mathbf{x})$. Figure 7(b) shows parameter space after having assigned all votes, the arrow indicates the vector $\tilde{v}$ estimated.

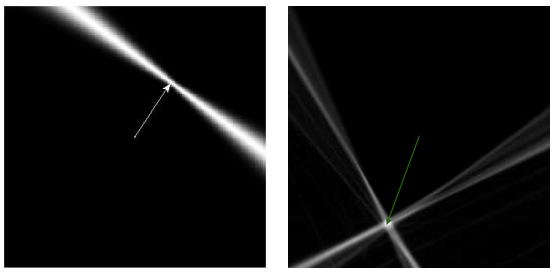

(a) (b)

Figure 7: (a) Neighborhood $\ell_{\mathbf{x}}(\mathbf{u})$ used to assign votes in parameter space. Vector represent $N(\mathbf{x})$. (b) Sum of votes in parameters space, the vector drawn is $\tilde{v}$.

5 EXPERIMENTAL RESULT

5.1 Algorithm Details

Given a window containing a blurred corner, we proceed as follows

- Define D_0, the set of considered pixels as $D_0 = \{\mathbf{x}\ s.t.\ ||\nabla I(\mathbf{x})|| > T\}$, where $T > 0$ is a fixed threshold. In such a way we exclude those pixels where image y is constant but gradient is non zero because of ξ and η.
- Estimate σ_η using the linear filtering procedure proposed in (Immerkær, 1996).
- Estimate Δ as $\Delta = |max(D_0) - min(D_0)| + 3 * \sigma_\eta$.
- Voting: $\forall \mathbf{x} \in D_0$ distribute votes in parameter space computing $\ell_{\mathbf{x}}(\mathbf{u})$ and adding them to the previous votes. The k parameter used in (11) is chosen between $[0.02, 0.04]$.
- The solution of (6), $\tilde{v}$, is the vector having endpoint in the most voted coordinates pair. Whenever several parameter pairs receive the maximum vote, their center of mass is selected as $\tilde{v}$ endpoint.
- To speed up the algorithm, we eventually consider gradient values only at even coordinate pairs.

5.2 The Experiments

In order to evaluate our approach we made several experiments, both on synthetic and real images.

5.2.1 Synthetic Images

We generate synthetic images according to (1), using a binary corner (like that of Section 2.2) taking y constantly equal to 0 at background and equal to 1 at corner pixels and with η and ξ having gaussian distribution. Motion parameters have been estimated on several images with values of the standard deviations $\sigma_\eta \in [0, 0.02]$ and $\sigma_\xi \in [0, 0.08]$. Blur was given by a convolution with a PSF v having direction 10 degrees and length 20 pixels in the first case and 70 degrees and 30 pixels in the second case. Figure 8 and Figure 9 show some test images and Table 1 and Table 2 present algorithm performances in terms of distance, in pixel unit, between the endpoints of the estimated, $\tilde{v}$, and the true displacement vector v, expressed as a percentage w.r.t psf length.
Comparing the first rows of Table 1 and Table 2, we notice the correlation produced by the blur on ξ samples, as expressed in equation (9). In fact, as the blur extent increases, the impact of ξ is reduced.

Table 1: Result on synthetic images: v has direction 10 degrees and length 20 pixels, $\sigma_\eta \in [0, 0.02]$ and $\sigma_\xi \in [0, 0.08]$.

$\sigma_\eta \mid \sigma_\xi$	0	0.02	0.04	0.06	0.08
0	1.94%	2.37%	1.67%	3.26%	5.40%
0.01	6.54%	2.98%	1.67%	4.21%	1.68%
0.02	4.14%	7.57%	5.40%	3.97%	3.35%

Table 2: Result on synthetic images: v has direction 70 degrees and length 30 pixels, $\sigma_\eta \in [0, 0.02]$ and $\sigma_\xi \in [0, 0.08]$.

$\sigma_\eta \mid \sigma_\xi$	0	0.02	0.04	0.06	0.08
0	1.95%	1.08%	1.95%	2.23%	0.98%
0.01	3.04%	0.31%	3.99%	1.43%	2.54%
0.02	9.39%	10.11%	6.55%	7.65%	7.50%

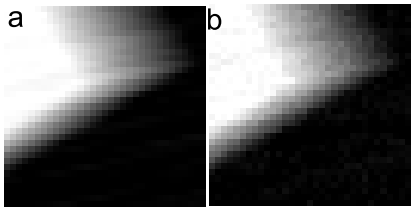

Figure 8: Synthetic test images used psf directed 10 degrees and length 20 pixels, in **a** $\sigma_\eta = 0$ and $\sigma_\xi = 0.08$, while in **b** $\sigma_\eta = 0.02$ and $\sigma_\xi = 0$.

5.2.2 Real Images

We perform two tests on real images[1]; in the first test we replace $y + \xi$ with a still camera picture, we blur it using a convolution with a PSF and we finally add gaussian white noise η. We take *house* as the original image and we manually select five squared windows of side 30 pixels at some corners. Figure 10 shows the original and the blurred *house* image (using psf with direction 30 degrees and length 25 pixels) and the analyzed regions. Figure 11 shows two vectors in pixel coordinates, the estimated $\tilde{v}$ (dashed line) and the vector having true motion parameters (solid line), for each selected region. Table 3 shows distance between the endpoints of the two vectors.

Table 3: Estimation error: distance between $\tilde{v}$ endpoint and displacement vector, expressed in pixels, on each image region r.

σ_η	r 1	r 2	r 3	r 4	r 5
0	2.07	2.75	3.19	1.87	2.04
0.01	0,32	6.91	3.52	2.64	4.58

We perform a second experiment using a sequence of camera images, captured according to the following scheme

- a still image, at the initial camera position.
- a blurred image, captured while the camera was moving.
- a still image, at the final camera position.

We estimated motion blur at some manually selected corners in the blurred image and we compare results

[1]Further images and experimental result are available at `http://www.elet.polimi.it/upload/boracchi`

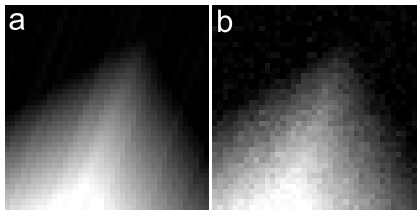

Figure 9: Example of synthetic test images used, psf was directed 70 degrees and length 30 pixels, in **a** $\sigma_\eta = 0$ and $\sigma_\xi = 0.08$, while in **b** $\sigma_\eta = 0.02$ and $\sigma_\xi = 0$.

Figure 10: Original and blurred house image. Blur have direction 30 degrees and 25 pixels length, regions analyzed are numbered.

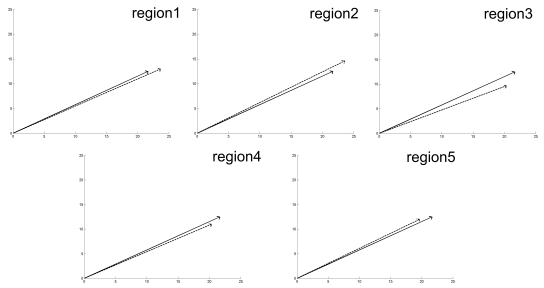

Figure 11: Displacement vectors $\tilde{v}$ estimated in selected regions of camera images. The solid line is the true displacement vector, while the dotted line represents the estimated vector $\tilde{v}$.

with the ground truth, given by matching corner found by Harris detector in the images taken at the initial and at the final camera position. Clearly, the accuracy obtained in motion estimation from a single blurred image is lower than that obtained with methods based on two well focused views. However preliminary results show good accuracy. For example, motion parameters estimated in region r 2 are close to the ground truth, even if the corner is considerably smooth, as it is taken from a common swivel chair. As Figure 13.2 shows, the votes in parameter space are more spread around the solution than in Figure 13.1, where the corner is close to the model of Section 2.2. Table 4 shows result using the same criteria of Table 3.
Results are less accurate than in previous experiments

because according to experimental settings, motion PSF could be not perfectly straight or not perfectly uniform, because of camera movement. This affects algorithm performances since it approximates motion blur to a vectorial PSF.

Table 4: Estimation error expressed in pixel unit on each image region r.

r 1	r 2	r 3	r 4	r 5
0.44	1.90	1.09	3.95	3.75

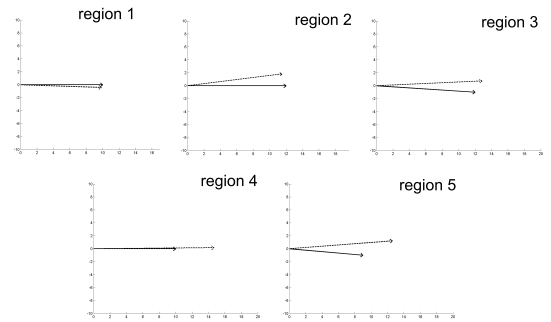

Figure 12: Displacement vectors $\tilde{v}$ estimated in camera images. In each plot, the solid line indicates the true displacement vector obtained by matching corners of pictures at initial and final camera position. Dotted line represents the estimated displacement vector $\tilde{v}$.

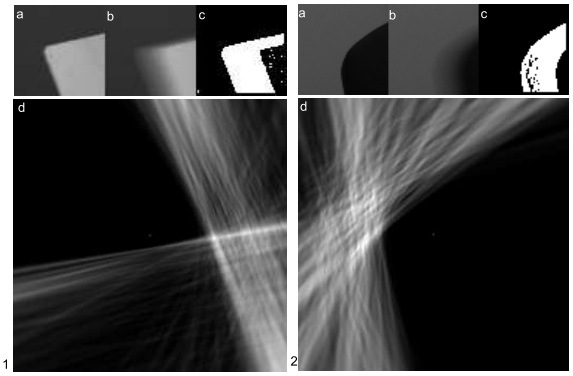

Figure 13: Figure **a** Original corner in image **b** blurred corner, **c** set D_0 of considered pixels and **d** votes in the space parameter.

6 ONGOING WORK AND CONCLUDING REMARKS

Results from the experiments, performed both on synthetic and natural images, show that the image at blurred corners has been suitably modelled and that the solution proposed is robust enough to cope with artificial noise and to deal with real images.
However, we noticed that there are only a few useful corners in real images. This is mostly due to background and corner non uniformity because of shadows, occlusions or because the original image itself shows significant intensity variations.
We are actually investigating a procedure to automatically detect blurred corners in a given image and to adaptively select image regions around them. In this paper we use squared regions but there are no restrictions on their shape, which could be adaptively selected to exclude background elements which would be considered in D_0. We believe that estimating blur on adaptively selected regions could significantly improve the algorithm performance on real images.
We are also investigating an extension of our algorithm to deal with corners which are moving like Figure 4 **b** or at least to discern which corners satisfy our image model.
Finally, we are looking for a criteria to estimate the goodness of an estimate, as up to now, we consider the value of the maximum voted parameter pairs.

REFERENCES

Bertero, M. and Boccacci, P. (1998). *Introduction to Inverse Problems in Imaging*. Institute of Physics Publishing.

Choi, J. W., Kang, M. G., and Park, K. T. (1998). An algorithm to extract camera-shaking degree and noise variance in the peak-trace domain.

Harris, C. and Stephens, M. (1988). A combined corner and edge detector.

Immerkær, J. (1996). Fast noise variance estimation.

Kawamura, S., Kondo, K., Konishi, Y., and Ishigaki, H. (2002). Estimation of motion using motion blur for tracking vision system.

Klein, G. and Drummond, T. (2005). A single-frame visual gyroscope.

Lin, H.-Y. (2005). Vehicle speed detection and identification from a single motion blurred image.

Lin, H.-Y. and Chang, C.-H. (2005). Automatic speed measurements of spherical objects using an off-the-shelf digital camera.

Mikolajczyk, K., Tuytelaars, T., Schmid, C., Zisserman, A., Matas, J., Schaffalitzky, F., Kadir, T., and Gool, L. V. (2005). A comparison of affine region detectors.

Rekleitis, I. (1996). Steerable filters and cepstral analysis for optical flow calculation from a single blurred image.

Yitzhaky, Y. and Kopeika, N. S. (1996). Identification of blur parameters from motion-blurred images.